Interrelation between swelling, mechanical constraints and reaction-diffusion processes in molecular responsive hydrogels

Eleonóra Parelius Jonášová[1], *Bjørn Torger Stokke*[1], *Victorien Prot*[2]
[1]*Biophysics and Medical Technology, Department of Physics, Norwegian University of Science and Technology, NO-7491 Trondheim, Norway*
[2]*Biomechanics, Department of Structural Engineering, Norwegian University of Science and Technology, NO-7491 Trondheim, Norway*

Abstract

The net swelling dynamics in molecular responsive hydrogels can be viewed as an integrated effect of discernible processes involving transport of actuating species, reaction with network components like destabilization of physical crosslinks or cleavage of network strands and concomitant network relaxation. Here, we describe a finite element modeling approach coupling these interdependent, underlying processes in hydrogels including oligonucleotide duplexes as physical crosslinks that can be destabilized by a particular molecule. These molecular responsive hydrogels based on acrylamide including either DNA or oligomorpholinos, a DNA analogue, as functional elements can be made with various content of ds-DNA or dsMO supported cross-links. The dsDNA or dsMO integrated in the hydrogel can be fabricated with ssDNA designed to competitively displace the connectivity of the dsDNA supported crosslinks, and similar for the MO hydrogels. The overall processes can be framed in a diffusion-reaction scheme. This process is dependent on the concentration of the diffusing species, their diffusion coefficients and their spatial coordinates. Thus, the reaction taking place in particular molecular responsive hydrogels is coupled with the deformations due to swelling and mechanical constraints undergone by the gel. Numerical examples show the importance of coupling reaction-diffusion with mechanical deformations for such gels. Finally, our model is compared to swelling experiments of hemi-spheroidal molecular responsive hydrogels bounded to an optical fiber. Parameters of the reaction-diffusion model were obtained by fitting the model to reported experimental data where molecular stimuli designed with different molecular parameters for the competitive displacement reaction were employed in the swelling experiments.

Keywords:

Finite element modeling, responsive hydrogels, reaction-diffusion, swelling

1 Introduction

Hydrogels are materials comprised of crosslinked polymers and water [1], thus having both solid-like and fluid-like properties. A rich plethora of polymers either from naturally existing components or synthesized ones are explored for hydrogels. Responsive hydrogels are a group within these soft materials able

to change their extent of swelling or other properties depending on environmental factors[2,3]. Stimuli can either be of generic nature such as temperature, light or pressure, or specific molecules for hydrogels tailormade to recognize these compounds and change their state accordingly[4–6]. Examples of molecular responsive hydrogels include e.g. antigen-antibody supported crosslinks in the hydrogel[7–9], tumor marker sensitive hydrogels based on combined lectin and antibody recognition[10], enzyme sensitive hydrogels[11,12], glucose sensitive hydrogels[13–15] and hydrogels with responsive character mediated by DNA structures[12,16–19]. Applications of molecular responsive hydrogels includes e.g. use as specific signal recognition and transducing elements in biosensing, adaptive materials in tissue engineering, and drug release materials[20,21].

While solvent/network diffusion and relaxation are dominating processes in the stimuli responsive hydrogels[22], the change of properties of the molecular responsive hydrogels additionally involve transport of the specific analyte, recognition event, and subsequent change induced in the network structure. Overall, these processes integrate with those discernible in the stimuli responsive hydrogel as a basis for the understanding of the overall effect. One example to indicate the particular molecules and processes in more detail is the specific response triggered in hydrogels that include DNA. Hydrogels based on acrylamide including DNA as a functional element initially reported by Nagahara and Matsuda[23], can be made with various content of dsDNA supported crosslinks, either only with these groups to support the crosslinked state, or alongside covalent ones[24–26]. The dsDNA integrated in the hydrogel can be designed with user specified base sequences to tailormake binding parameters and susceptibility to nucleases or Crispr CAS cleaving the dsDNA, or complementary ssDNA designed to competitively displace the connectivity of the dsDNA supported crosslinks[12,19].

The overall processes can be framed in a diffusion-reaction scheme modified to also include the changes in local swelling as may occur. For the DNA modified hydrogels, the experiments are typically initiated with an initial constant concentration of the molecular stimuli in an aqueous immersing solution outside the hydrogel, thus also setting up a step function as the initial condition for the diffusion-reaction process. The initial concentration gradient drives the transport, and when the molecular stimuli is reaching dsDNA within the hydrogel, it will bind according to the molecular properties. The concomitant effects are both the reduction of the local concentration of the diffusible molecular stimuli, the reaction eventually leading to a reduction of the local crosslink density, concomitant swelling and, depending on whether the reaction is retaining (ssDNA) or not retaining (enzyme) the stimuli, eventually return the molecular stimuli to the pool of diffusible molecules. Thus, there are coupled processes in the diffusion-reaction scheme, where spatiotemporal changes in the various species depend on the actual parameter values. Thombre and Himmelstein[27] and Joshi and Himmelstein[28] proposed a mathematical model combining diffusion and reaction for predicting drug release from a poly (ortho ester) system. Other groups[29–31] have used similar reaction-diffusion models to study drug delivery systems and transport in hydrogels. In addition, Parlato and Murphy[32] provided a comparison of the transport of soluble molecules between synthetic hydrogels and extracellular matrix. These models are dependent on the concentration of the diffusing species, their corresponding diffusion coefficients, their spatial coordinates and their net sum of synthesis and degradation rate. Combined with these facets, Fick's second law is used to describe transient diffusion, i.e., when the concentration within the diffusion volume changes with respect to time and space.

In this work, we employ a reaction-diffusion model to describe spatiotemporal dynamics of molecular responsive hydrogels. The reaction taking place in these gels may lead to a reduction in local crosslink density thus inducing a local change in mechanical properties also including deformations, i.e., swelling. As the reaction-diffusion process is dependent on the spatial position of ssDNA, it may have to be coupled with the mechanical finite deformations.

We have previously reported on determination of various parameters in a reaction-diffusion scheme based on experimentally determined spatiotemporal changes in the concentration of ssDNA as the molecu-

lar stimulus in hydrogels with incorporated dsDNA as crosslinks. As a first approximation, it was assumed that changes in hydrogel swelling occurring in this process could be ignored. The limited extent of swelling for the particular hydrogel designs used in that work was used as an argument to simplify the modeling approach in that case. In the present work, we also take into account changes in the swelling state of the hydrogel occurring on changes in crosslink density, thus relaxing the previous assumption. The swelling is also developing locally while the interrelated processes proceed, as also will be evident in the following.
This is achieved by implementing our reaction diffusion model into the Finite Element code `ABAQUS`. Details on the implementation are given. We compare our Finite Element implementation of the reaction-diffusion model to results obtain with a built-in MATLAB function. Then, a simple numerical example is developed for coupling of uniaxial swelling and reaction-diffusion for which results obtained with MATLAB and `ABAQUS` are also compared. In addition, several numerical examples are presented to illustrate the influence of swelling and initial geometries on the reaction diffusion process. Finally, our model is fitted to previously reported experimental data to identify the parameters of the reaction-diffusion model.

2 Methods

2.1 Aspects of dsDNA-co-AAm and dsMO-co-AAm hydrogels

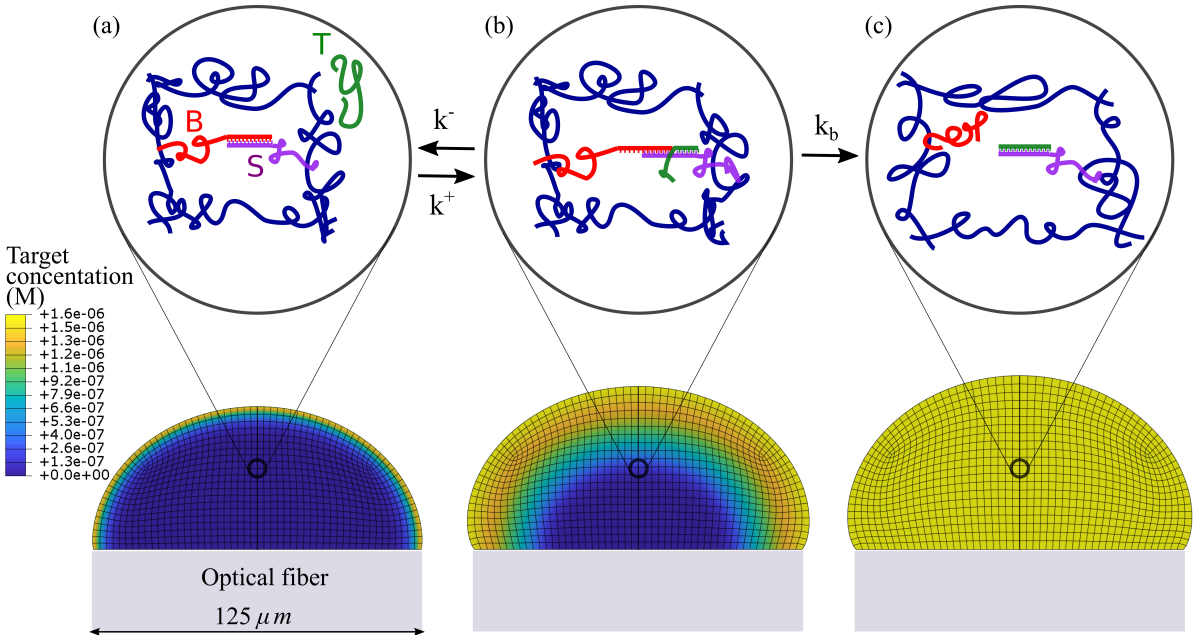

Figure 1: . Schematic illustration of the DNA-polyacrylamide hydrogel network and the process of toehold-mediated strand displacement. The target DNA (T) binds to (rate constant k^+) and dissociates (rate constant k^-) from the hybridized sensing-blocking SB dsDNA in the hydrogels (a,b), and a bound target DNA undergoes branch migration with a rate k_b to dissociate the SB duplex (b,c). The snapshots of the Finite Element model show that as the diffusing front Target T advances into the hydrogels, SB duplexes open thus reducing its crosslink density and causing swelling. S-Sensing, B-Blocking, T-Target

The modeling developed here aims to provide more detailed description of the stimuli-responsive process in hydrogels where a toehold mediated strand displacement eventually yielding crosslink destabilization, is mechanistic (Fig. 1). This general molecular responsive process is realized for acrylamide based hydrogels where either dsDNA or dsMO are included as physical crosslinks that can be dissociated by a specific molecule. In the following more detailed description we refer only to dsDNA based crosslinks for simplicity. The dsDNA-co-Aam hydrogels covalently attached to the end of an optical fiber supporting high resolution determination of overall changes of the optical lengths of the hydrogel were synthesized. The dsDNA supported crosslinks with user selected base pair (bp) sequence were termed with the two ssDNA as either blocking (B) or sensing (S) strand, where a total of 10 bp (14 bp for the MO) stabilizing the duplex. A third type of ssDNA, referred to as target (T) DNA, was designed with a longer bp complementarity to the sensing ssDNA, and the excess complementarity compared to the S strand is the toehold. The hydrogel swelling processes when exposed to target ssDNA with user selected toeholds of 3 and 7 base pairs, T3 and T7 target DNA, respectively, were included in this analysis of the DNA-co-AAm and toehold lengths of 2 and 10 basepairs for the MO-co-AAm hydrogels. In the process of toehold mediated strand displacement, the target DNA binds to the SB dsDNA in the toehold region yielding a TSB DNA triplex, followed by strand displacement of the S ssDNA from B ssDNA, ending up with a TS dsDNA duplex (Fig. 1). At difference with the B ssDNA, the target DNA is linked to the polymer network, thus yielding an overall effect of destabilizing the DNA mediated crosslink at completion of the competitive strand displacement. Fluorescently labelled target DNAs were included to support spatiotemporal determination of target DNA following initiation of the experiment by adding the target to the aqueous immersing solution.

2.2 Constitutive equations

2.2.1 Free energy function and Cauchy stress tensor

The constitutive modeling of hydrogel behavior applied herein is based on the work by Hong *et al.*[33,34], Kang and Huang[35], and Toh *et al.*[36]. The free-energy function for the hydrogel is assumed to originate from the additive contributions of stretching of the polymer network and mixing of the polymer and the solvent molecules[37–39]

$$U(\mathbf{F}, C_S) = \frac{1}{2}Nk_BT(I_1 - 3 - 2\ln J) + \frac{kT}{v}\left(vC_S \ln\left(\frac{vC_S}{1+vC_S}\right) + \frac{\chi vC_S}{1+vC_S}\right), \quad (1)$$

where N is the number of polymeric chains per reference volume (i.e. the crosslink density), k_BT is the temperature in the unit of energy, $\mathbf{F}$ is the deformation gradient tensor, $I_1 = \mathrm{tr}\mathbf{b}$ is the first invariant of the left Cauchy-Green tensor $\mathbf{b} = \mathbf{F}\mathbf{F}^{\mathrm{T}}$, $J = \det\mathbf{F}$ is the volume ratio of the material, v is the volume per solvent molecule, C_S is the nominal concentration of solvent molecules, and χ is the Flory-Huggins parameter.

By assuming that both the polymer network and the solvent molecules retain their volumes through the swelling process, we find that the volume increase of the gel only can come from an increase in the number of solvent molecules inside the gel, hence we can write

$$J = \det \mathbf{F} = 1 + vC_S. \tag{2}$$

Further, to enable implementation for the finite element method, we introduce the free-energy function $\hat{W}$ using a Legendre transformation as

$$\hat{U}\left(\mathbf{F}, \mu\right) = U\left(\mathbf{F}, C_S\right) - \frac{\mu}{v}\left(J - 1\right) \tag{3}$$

and hence ensure the deformation gradient $\mathbf{F}$ and the chemical potential μ to be the two independent variables of the model. The Cauchy stress tensor $\boldsymbol{\sigma}$ can then be obtained from the free-energy potential function as

$$\boldsymbol{\sigma} = \frac{1}{J}\frac{\partial \hat{U}\left(\mathbf{F}, \mu\right)}{\partial \mathbf{F}}\mathbf{F}^{\mathrm{T}} = Nk_BT\left(J^{-1}\mathbf{b} + \frac{1}{Nv}\left(\ln\frac{J-1}{J} + \frac{1-Nv}{J} + \frac{\chi}{J^2} - \frac{\mu}{k_BT}\right)\mathbf{1}\right), \tag{4}$$

where $\mathbf{1}$ is the second-order identity tensor.

As the chemical potential is singular in the dry state of the hydrogel K_0, an intermediate configuration K_1 is introduced. K is the current configuration. Let $\mathbf{x}$ denote the present (deformed) position in K in rectangular cartesian coordinates of a material particle that occupied the location $\mathbf{X}$ in K_0. The deformation gradient $\mathbf{F} = \frac{\partial \mathbf{x}}{\partial \mathbf{X}}$ maps K_0 into K. Additionally, a multiplicative decomposition of the deformation tensor $\mathbf{F}$ is employed such as $\mathbf{F} = \mathbf{F}_1\mathbf{F}_0$. $\mathbf{F}_0$ maps K_0 into K_1, and $\mathbf{F}_1$ maps K_1 into K, as illustrated in Figure 2. In the intermediate configuration K_1, the gel is assumed stress-free and in a homogeneous state of isotropic strain such that $\mathbf{F}_0 = \lambda_0\mathbf{I}$. In the present study, all finite element simulations start in the intermediate configuration K_1 with a known homogeneous state of isotropic strain. The value of the chemical potential μ in K_1 is found by solving $\boldsymbol{\sigma} = \mathbf{0}$. The constitutive model described above was implemented in the FE code `ABAQUS` as a Fortran subroutine UMAT[40].

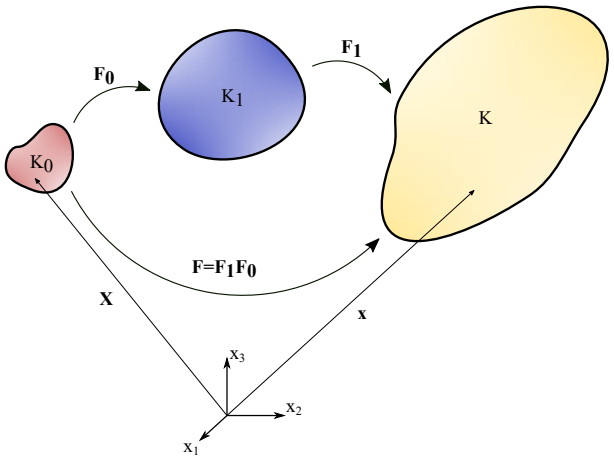

Figure 2: Illustration of the reference, intermediate, and current configurations. All finite element simulations herein start in the intermediate configuration.

2.2.2 Mathematical model for reaction-diffusion process of target T DNA into the hydrogel

The conservation equation for a chemical species subject to reaction and diffusion can be written with respect to the current coordinates $\mathbf{x}$:

$$\frac{\partial c(\mathbf{x},t)}{\partial t} + \frac{\partial q_k}{\partial x_k} = s(\mathbf{x},t), \tag{5}$$

$$\text{with} \qquad q_i = -D\frac{\partial c(\mathbf{x},t)}{\partial x_i}. \tag{6}$$

$\mathbf{q}$ is the spatial flux vector and is related to the deformed surface da with outer normal $\mathbf{n}$ in the current configuration K. D is the diffusion coefficient of the free target T in the hydrogel. $c(\mathbf{x},t)$ is the molar concentration of the free target T in the current configuration (i.e. the true concentration). Here, the variable s is a sink term expressed per current volume. When deformations occurs due to swelling or external loads, eq.(5) must be solved accounting for the variations of the spatial coordinates with respect to time. It may be useful to rewrite eq.(5) with respect to the material coordinates $\mathbf{X}$. The material description the reaction-diffusion process reads as follows:

$$\frac{\partial C(\mathbf{X},t)}{\partial t} + \frac{\partial Q_K}{\partial X_K} = S(\mathbf{X},t), \tag{7}$$

$$\text{with} \qquad Q_k = -M_{KL}\frac{\partial C(\mathbf{x},t)}{\partial X_L}. \tag{8}$$

The nominal flux vector $\mathbf{Q}$ is related to the undeformed surface dA with outer normal $\mathbf{N}$ in the dry configuration K_0. $\mathbf{M}$ is the mobility tensor. $C(\mathbf{X},t)$ is the nominal concentration of the free target T such as $C(\mathbf{X},t) = Jc(\mathbf{x},t)$. S is defined per reference volume and $S(\mathbf{X},t) = Js(\mathbf{x},t)$. The relation between the undeformed area dA in K_0 and the corresponding deformed area da in K is given by the formula: $JN_k dA = F_{iK} n_i da$. The number of free target T crossing the material element per unit time can be written in two equivalent ways, in K or K_0:

$$q_i n_i da = Q_K N_K dA \tag{9}$$

Consequently, this leads to the following relation between the true flux $\mathbf{q}$ and the nominal flux $\mathbf{Q}$:

$$q_i = \frac{F_{iK}}{J} Q_K \tag{10}$$

Using,

$$\frac{\partial C(\mathbf{x},t)}{\partial X_K} = \frac{\partial C(\mathbf{x},t)}{\partial x_i}\frac{\partial x_i}{\partial X_K} = \frac{\partial C(\mathbf{x},t)}{\partial x_i} F_{iK}, \tag{11}$$

the relation between the mobility tensor $\mathbf{M}$ and the diffusion coefficient D reads:

$$\mathbf{M} = D\mathbf{F}^{-1}\mathbf{F}^{-\mathrm{T}}. \tag{12}$$

The spatial formulation eq.(5) and the material formulation eq.(7) are equivalent, and one choose either of these that is relevant for a given solver. In the FE solver `ABAQUS`, the reaction diffusion model has to be given in the form presented in eq.(5). However, with the pdepe Matlab function the formulation described by eq.(7) is more suitable as this solver uses a fixed spatial mesh.

In this study, we use

$$s(\mathbf{x},t) = -k^+ c m_t + k^+ c m_c + k^+ c m_0 + k^- m_c \tag{13}$$

$$\frac{\partial m_c}{\partial t} = k^+ c m_t - k^+ c m_c - k^+ c m_0 - k^- m_c - k_b m_c \tag{14}$$

$$\frac{\partial m_0}{\partial t} = k_b m_c, \tag{15}$$

m_f, m_c and m_0 are the true concentrations of the free binding sites, the 3-strand complexes and the open crosslinks. The total molar concentration m_t of available binding sites is defined such as $m_t = m_f + m_c + m_0$. The binding of the target to the hydrogel-bound strands and the subsequent crosslink opening can be modelled as a two-step process characterized by the binding constant k^+, the dissociation constant k^- and the constant of junction point migration k_b.

2.2.3 Dynamics of the crosslink density

The description of the dynamics of the total crosslink density, N, take into account that the overall N consists of two contributions:

- One from the covalent, permanent crosslinks (Bis), N_{bis}
- One from the dsDNA supported crosslinks, N_{dsDNA}

These are additive since the strain–energy contribution is linear with respect to N. Thus,

$$N = N_{bis} + N_{dsDNA}. \tag{16}$$

The N_{dsDNA} is changing due to the interaction/reaction with the target DNA, thus locally reducing the crosslink density; resulting in swelling.
While the elastic term is the main contributing factor to limit the extent of swelling, the Donnan term is a larger driving factor for increased swelling volume (at the given charge densities). Although there are changes also in the Donnan term on binding of target DNA to the embedded DNA, the data for T7b as compared to T7 target indicate that the altered charge density associated with the target DNA binding are less than the crosslink opening. As a first approximation: only consider changes in crosslink density term:

$$N_{dsDNA}(\mathbf{x},t) = N_{dsDNA}(\mathbf{x},t_0) - \beta m_0(\mathbf{x},t), \quad \beta = \frac{\gamma N_{dsDNA}(\mathbf{x},t_0)}{m_0(\mathbf{x},t\to+\infty)}, \quad 0 \le \gamma \le 1 \tag{17}$$

$$\frac{\partial N}{\partial t} = -\beta \frac{\partial m_0}{\partial t} = -\beta k_b m_c. \tag{18}$$

The swelling process due to the opening of the dsDNA supported crosslinks is illustrated in Figure 1.

2.2.4 Diffusion coefficient

As a first approximation, D the diffusion coefficient of the target T in the gel may be assumed constant. However, the diffusivity of a solute in a hydrogel may depend on the crosslinking density, the size of the

solute and the polymer volume fraction.[41–43]. Several mathematical models derived to explain and predict solute diffusion in hydrogels. Amsden[44] provides a review of these mathematical expressions. In this work, we use a hydrodynamic description of solute transport through gels based on the Stokes–Einstein equation for solute diffusivity. We adopt the equation proposed by Cukier[45] for the diffusion constant of a solute in homogeneous hydrogels:

$$D = D_0 \exp\left(-k_c a_h \varphi^{0.75}\right), \tag{19}$$

where k_c is an undefined constant for a given polymer-solvent system, φ is the polymer volume fraction of the gel, a_h is the hydrodynamic radius of the species diffusing and D_0 is is the diffusion coefficient in the solution that may be calculated with the Stokes–Einstein equation. k_c is determined from the initial values of D and φ in Configuration K_1. In the present work, D_0 is assumed equal to 155 $\mu m^2 s^{-1}$ for the 18 bp DNA target probe as based on the determination of diffusion properties for ssDNA as a function of number of bp's[46] . Thus, D is a solution-dependent material property: variations of the distance between crosslinks induce local alteration of the diffusion coefficient. The USDFLD user-subroutine is used to implement eq.(19) in the FE solver `ABAQUS`.
In this study, the diffusion constant D is either constant or a function of the polymer volume fraction φ as described in eq.(19).

2.2.5 FE implementation of Reaction-Diffusion process of the free target

Eq.(5) is solved directly by the `ABAQUS` FE solver. However, its right-hand side $s(\mathbf{x}, t)$ (see relation (13)) needs to be implemented. To this end, we used the user-subroutine HETVAL.
Let's consider a time increment n of size Δt. We use a backward Euler method to solve eqs.(14) and (15) for the true concentrations of 3-strand complexes m_c and open crosslinks m_0, respectively:

$$\frac{m_c^{n+1} - m_c^n}{\Delta t} = k^+ c^{n+1} m_t - k^+ c^{n+1} m_c^{n+1} - k^+ c^{n+1} m_0^{n+1} - k^- m_c^{n+1} - k_b m_c^{n+1} \tag{20}$$

$$\frac{m_0^{n+1} - m_0^n}{\Delta t} = k_b m_c^{n+1}, \tag{21}$$

where the superscripts n and $n+1$ denote the values of the corresponding concentrations at the beginning and at the end of the time increment n, respectively. Eq.(21) leads to:

$$m_0^{n+1} = k_b m_c^{n+1} \Delta t + m_0^n. \tag{22}$$

Using eq.(22) into eq.(20) gives the following expression for the concentration of 3-strand complexes m_c^{n+1},

$$m_c^{n+1} = \frac{m_c^n + k^+ c \Delta t (m_t - m_0^n)}{1 + k^+ c \Delta t + k^- \Delta t + k_B \Delta t + k^+ k_b c \Delta t^2}. \tag{23}$$

The numerical procedure used to compute $s(\mathbf{x}, t)$ is summarized in the following algorithm:

1: **set:** $n = 0$
2: **initialization:** set c^0, m_c^0, m_0^0 as boundary conditions
3: **while** Analysis is not completed
4: **Inputs:** Δt, c_{n+1} from the FE solver
5: **compute:** m_c^{n+1} using eq.(23)
6: **compute:** m_0^{n+1} using eq.(22)

7: **Output:** $s = -k^+c^{n+1}m_t + k^+c^{n+1}m_c^{n+1} + k^+c^{n+1}m_0^{n+1} + k^-m_c^{n+1}$ (eq.(13))
8: **set:** $n = n + 1$
9: **go to** 4
10: **end while**

2.3 Experimental data

The numerical modeling in the present paper addresses the importance of swelling of molecular responsive hydrogels, where data reported previously for DNA-co-AAm and Morpholino-co-AAm hydrogels[47,48] serve as the proof of concept. In the fit to the experimental data, we employ the spatiotemporal data for the molecular stimuli (either a ssDNA or Morpholino) as they are transported, bind and dissociate physical crosslinks, and concomitant changes in extent of local swelling. An important facet of this is that the molecular stimuli are retained bound to the open crosslinks, according to its association constant, also after the crosslink opening, thus giving an observable signal that is aggregate of more than one state.

The experimental procedure for the preparation of these molecular stimuli responsive hydrogels is described more in detail in the supplementary, while we here summarize briefly the experimental setup and post-processing of the data. The reader is referred to the aforementioned publications for further details.

A quasi-hemispherical hydrogel is prepared at the end face of an optical fiber (diameter of 125 μm) in order to facilitate an interferometric size monitoring. However, in order to study the spatiotemporal distribution of the various target molecules in the hydrogels, confocal laser scanning microscopy (CLSM) is employed for spatiotemporal monitoring of the target molecules which are tagged with a fluorescent dye for this purpose. A small part of the fiber with the hydrogel on its end faced was pinched off using tweezers and glued to a bottom of glass bottom microwell dish (p35G-1.5-10-C, MatTek) (Figure 3(a)). Buffer solution was added to allow for the hydrogel to equilibrate. At the start of the image acquisition using the CLSM, an aliquot of the target stock solution was added to the dish to a final target concentration of 20 μM. Time lapse imaging was then performed at 22 °C by CLSM (Zeiss LSM800) with a 40x, NA = 1.2 water immersion objective, optical slice thickness of 0.9 μm). An image was acquired every minute, starting 10-40 s after adding the target to the aqueous immersing solution of the hydrogel thus initiating the reacion-diffusion process. The image plane was parallel to the glass dish and passed through the middle of the hydrogel at depth of approx. 62 μm.

CLSM micrographs (an examples is shown in Figure 3(b)) were processed using custom Matlab scripts. First, intensity profiles were extracted from images over several lines from a circular sector spanning 20 ° around the long axis of the fiber with a step of 0.5° (circular sector depicted in Figure 3(a) and extracted intensity profiles seen in white in Figure 3(b)). The average of these profiles was used for further analysis (black profile in Figure 3(b)). The profile was then smoothed by a Savitzky-Golay filter and normalized so that the intensity of the immersing solution was 1 for T2, T3, T7 and T10 (target oligos binding to the hydrogel) and so that the maximum intensity within the hydrogel was 1 for T0 (a target DNA that did not bind to the hydrogel and was used as reference). The resulting intensity profiles are referred to as I_{TX} where TX, X = 0, 2, 3, 7 or 10, denotes the particular target molecule. An example of a series of normalized fluorescence intensity profiles is depicted in Figure 3(c).

The close proximity of the glass optical fiber to the hydrogel during imaging leads to a decrease in the observed fluorescence intensity in the vicinity of the fiber due to lateral step changes in the refractive in-

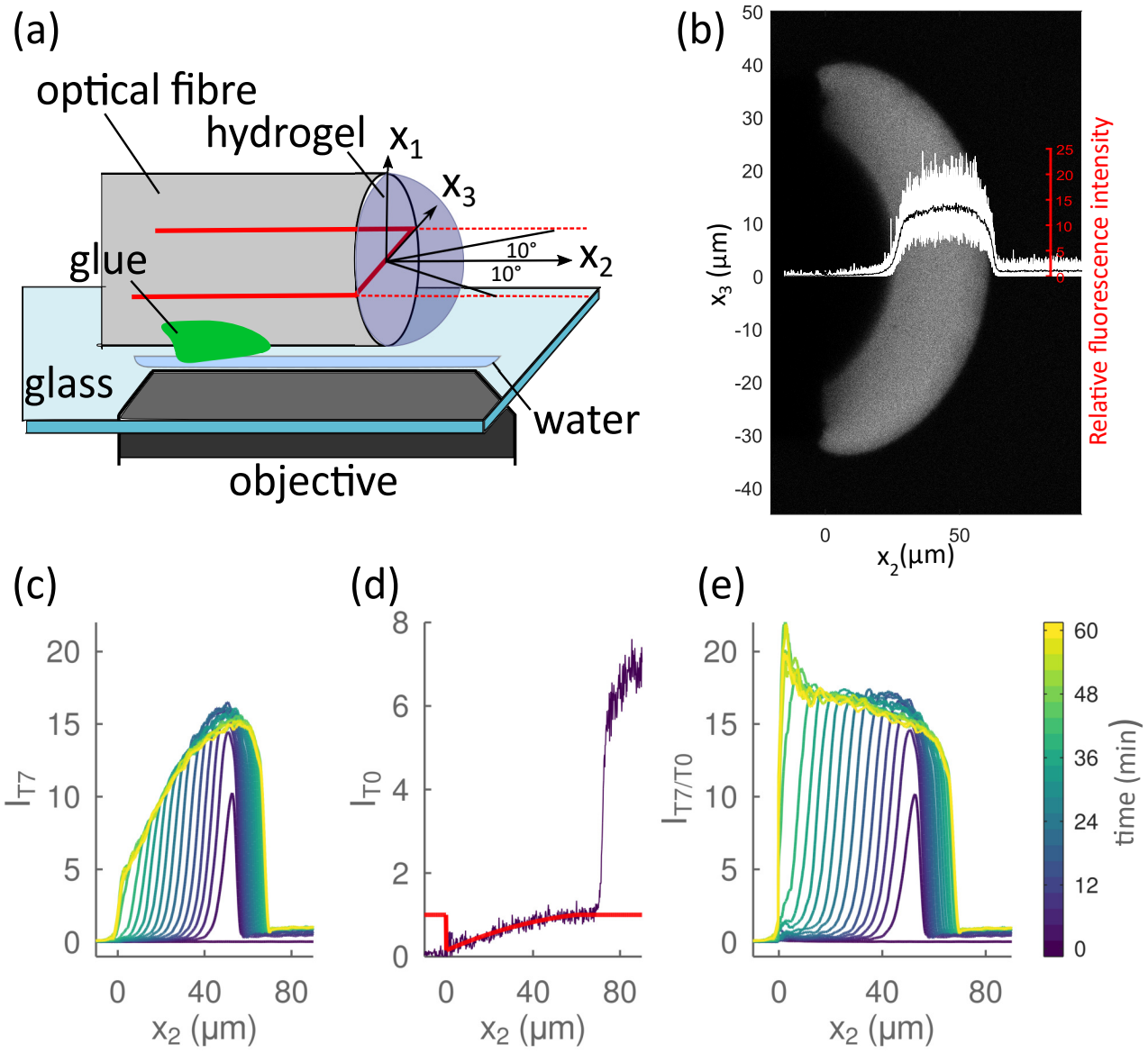

Figure 3: (a) Schematics of a hydrogel at the end face of an optical fibre, as it is imaged using a confocal laser scanning microscope. The imaging started after adding a solution of fluorescently labeled target to the glass well. The micrographs were acquired in a plane shown in red. Subsequently, intensity profiles were extracted from the micrographs within a circular sector also depicted here. (b) An example of a micrograph depicting the detected fluorescence from a target DNA T7. The image is taken at an intermediate state before equilibrium was reached. As overlay, intensity profiles extracted within the circular sector (as seen in (a)) are shown in white and their average is plotted in black. The fibre end face is located at $x_2 = 0$ (c) The fluorescence intensity profiles I_{T7} normalized such that the intensity of the surrounding solution is 1. A profile is shown for every third minute. (d) In purple, intensity profile of the nonbinding target T0 (IT0) inside and outside a hydrogel, smoothed and normalized so that the maximum intensity within the hydrogel is 1. (e) Intensity profiles I_{T7} from (c) divided by a reference profile acquired from T0 (d) to obtain an estimate of the relative concentration of the target $I_{T7/T0}$. The fiber end face is located at $x_2 = 0$.

dex[49]. This loss of fluorescence is an optical effect and does not represent a decrease in fluorophore concentration. Estimates of the spatiotemporal evolution of the target concentrations were obtained using a reference intensity profile I_{T0} for each individual hydrogel[47,49] (reference profile seen in Figure 3(d)). Since T0 does not bind to the hydrogel, its concentration throughout the hydrogel can be assumed constant. The concentration of the target relative to its concentration in the immersing solution (in 3C)(c) referred to as relative concentration profile $I_{\mathrm{TX/T0}}$) is then obtained by dividing the intensity profile I_{TX} by its corresponding reference profile I_{T0}. The relative concentration $I_{\mathrm{TX/T0}}$ and the known concentration of the target in the immersing solution is then used to estimate the total concentration of the target within the hydrogel (i.e. both free and bound target molecules).

The peak observed at low x_2 values in $I_{\mathrm{T7/T0}}$ (Figure 3(e)) is caused by the correcting procedure, which is sensitive to small misalignments in the position of the edge of the fiber in the main and the reference profile. The precise position of the edge is difficult to estimate due to the low fluorescence intensity in the immediate vicinity of the fibre and the nonzero confocal volume[49].

3 Numerical investigations of reaction diffusion, swelling, constraints and geometry

In this section, the finite element implementation presented in this work is compared with the MATLAB *pdepe* function for radial diffusion in a sphere where swelling is ignored (Section 3.1) and for longitudinal diffusion in a circular cylindrical hydrogel where swelling is accounted for (Section 3.2). In Sections 3.3 and 3.4, the influence of swelling, initial spheroidal geometries and mechanical constraints are investigated.
For all finite element analyses reported herein, the models are axisymmetric and meshed with four-noded elements (CAX4T `ABAQUS` type). Coupled temperature-displacement transient procedures are used with the `ABAQUS`\Standard solver.
The parameters used for reaction-diffusion and the hydrogel are reported in Table 1. Note that in this section the diffusion parameter D is constant.

Table 1: numerical values of the parameters used in Section 3

reaction-diffusion parameters		
Diffusion coefficient	$D(\varphi = 0.045)$	37.5 $\mu\mathrm{m}^2\mathrm{s}^{-1}$
Binding constant	k_+	500 $\mathrm{M}^{-1}\mathrm{s}^{-1}$
Dissociation constant	k_-	0.02 s^{-1}
Constant of junction point migration	k_b	1000 s^{-1}
Available binding site concentration	m_t	0.006 M
Outer free target concentration	c_{out}	10^{-5} M
hydrogel parameters		
Permanent crosslink density	$N_{bis}v$	0.00044
Initial dsDNA supported crosslink density	$N_{dsDNA}v$	$\frac{2}{3}N_{bis}v$
see eq.(17)	γ	0.7
Flory–Huggins parameter	χ	0.45
Initial swelling ratio	λ_0	2.8

3.1 Reaction-Diffusion into a spherical hydrogel

In this section, swelling is ignored. We consider a spherical gel of outer radius R submerged in an external solution with $c = 0$. The sphere is at equilibrium when at time t=0, the concentration of free target at the boundary of the gel in contact with the external solution is changed to $c = c_{out}$. For diffusion within a radially symmetric sphere the true concentration $c(r,t)$ as a function of time and current radial position r, is given as:

$$\frac{\partial c(\tilde{r},t)}{\partial t} = \frac{1}{\tilde{r}^2}\frac{\partial}{\partial \tilde{r}}\left(\tilde{r}^2\alpha\frac{\partial c(\tilde{r},t)}{\partial \tilde{r}}\right) + s(\tilde{r},t), \quad 0 \le \tilde{r} \le 1, \text{with } \tilde{r} = \frac{r}{R}, \tag{24}$$

$$\text{with} \quad s(\tilde{r},t) = -k^+cm_t + k^+cm_c + k^+cm_0 + k^-m_c, \tag{25}$$

$$\frac{\partial m_c}{\partial t} = k^+cm_t - k^+cm_c - k^+cm_0 - k^-m_c - k_bm_c, \tag{26}$$

$$\text{and} \quad \frac{\partial m_0}{\partial t} = k_bm_c, \tag{27}$$

where $\alpha = \frac{D}{R^2}$. The following initial conditions are used:

$$c(\tilde{r},t=0) = \begin{cases} 0 & \text{if } 0 \le \tilde{r} < 1 \\ c_{out} & \text{if } \tilde{r} = 1 \end{cases}, \tag{28}$$

$$m_c(\tilde{r},t=0) = 0 \quad \text{if } 0 \le \tilde{r} \le 1, \tag{29}$$

$$m_0(\tilde{r},t=0) = 0 \quad \text{if } 0 \le \tilde{r} \le 1. \tag{30}$$

In addition, the following boundary conditions are used for $t \ge 0$:

$$\frac{\partial c(\tilde{r}=0,t)}{\partial \tilde{r}} = 0 \tag{31}$$

$$c(\tilde{r}=1,t) = c_{out} \tag{32}$$

$$\frac{\partial m_c(\tilde{r}=0,t)}{\partial \tilde{r}} = 0 \tag{33}$$

$$m_c(\tilde{r}=1,t) = 0 \tag{34}$$

$$\frac{\partial m_0(\tilde{r}=0,t)}{\partial \tilde{r}} = 0 \tag{35}$$

$$m_0(\tilde{r}=1,t) = 0 \tag{36}$$

Herein, the system of partial differential equations described by eqs.(24-27) and the corresponding initial and boundary conditions described above is solved for the different concentrations numerically in two ways: first, using the *pdepe* MATLAB function where eqs.(24-27) are directly implemented and second using the FE element solver `ABAQUS` where the formulation described in Section 2.2.5 is used.
Figure 4 shows the concentrations c, m_c, m_0 along the normalized radius $\tilde{r}$ of a sphere obtained using the *pdepe* MATLAB function and the FE element solver `ABAQUS` against time. As can been seen, the computed concentrations from both solvers are in excellent agreement.

3.2 Coupling of uniaxial swelling and reaction-diffusion

In this section, we consider a circular cylindrical hydrogel (see Figure 5). Its upper surface is in contact with an external solution with $c = 0$ and the cylinder is constrained in its the lateral directions. The gel

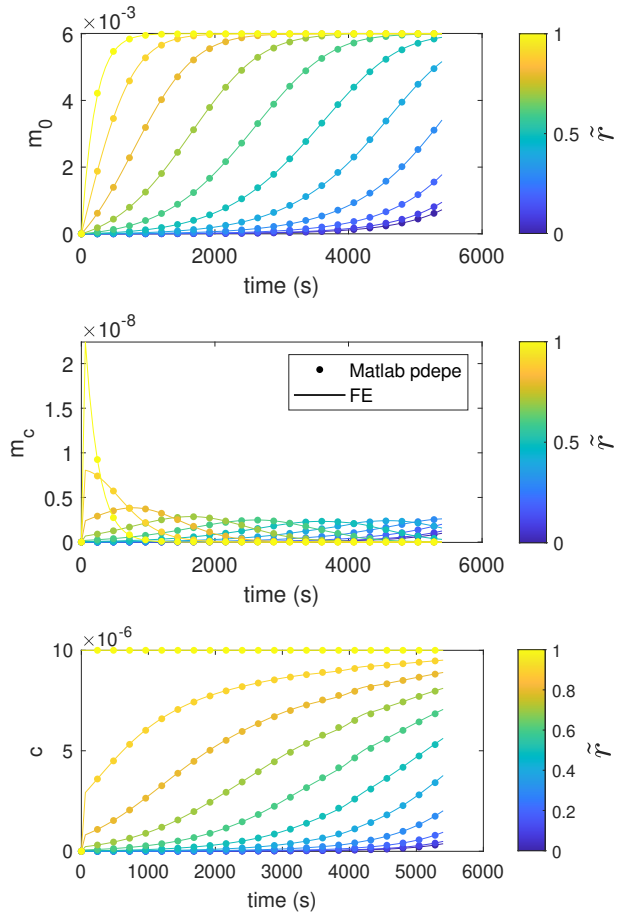

Figure 4: Concentrations c, m_c, m_0 (M) along the normalized radius $\tilde{r}$ of a sphere obtained using the *pdepe* MATLAB (circles) function and the FE element solver `ABAQUS` (solid lines) against time.

can freely swell in its longitudinal direction. Initially, the gel is at equilibrium in configuration K_1 in a state of isotropic swelling and has a radius R_1 (see Figure 5) and height H_1. Thus, the deformation gradient is $\mathbf{F} = \mathbf{F}_0 = \lambda_0 \mathbf{1}$. We define 1 and 2 as the lateral coordinates and 3 as the longitudinal coordinate. At time t=0, the concentration of free target at the upper surface in contact with the external solution is changed to $c = c_{out}$ and the gel starts swelling. The deformation gradient at any particle in the gel takes the following form in this coordinate system:

$$\mathrm{F} = \begin{bmatrix} \lambda_0 & 0 & 0 \\ 0 & \lambda_0 & 0 \\ 0 & 0 & \lambda_0 \lambda \end{bmatrix}. \tag{37}$$

Namely, the principal stretches of this hydrogel are $\lambda_1 = \lambda_2 = \lambda_0$ and $\lambda_3 = \lambda_0 \lambda$ and the Jacobian of the deformation is $J = \lambda_0^3 \lambda$. In addition, we assume that the gel is free to deform in the 3-direction. Therefore, this gel is in plane stress state with the Cauchy stress components $\sigma_{i3} = 0$ (with $i = 1, 2, 3$). Using $\sigma_{33} = 0$, we obtain the following relation:

$$0 = \frac{\lambda}{\lambda_0} + \frac{1}{vN}\left(\ln\left(\frac{{\lambda_0}^3\lambda - 1}{{\lambda_0}^3\lambda}\right) + \frac{1 - vN}{{\lambda_0}^3\lambda} + \frac{\chi}{{\lambda_0}^6\lambda^2} - \frac{\mu}{k_B T}\right) \tag{38}$$

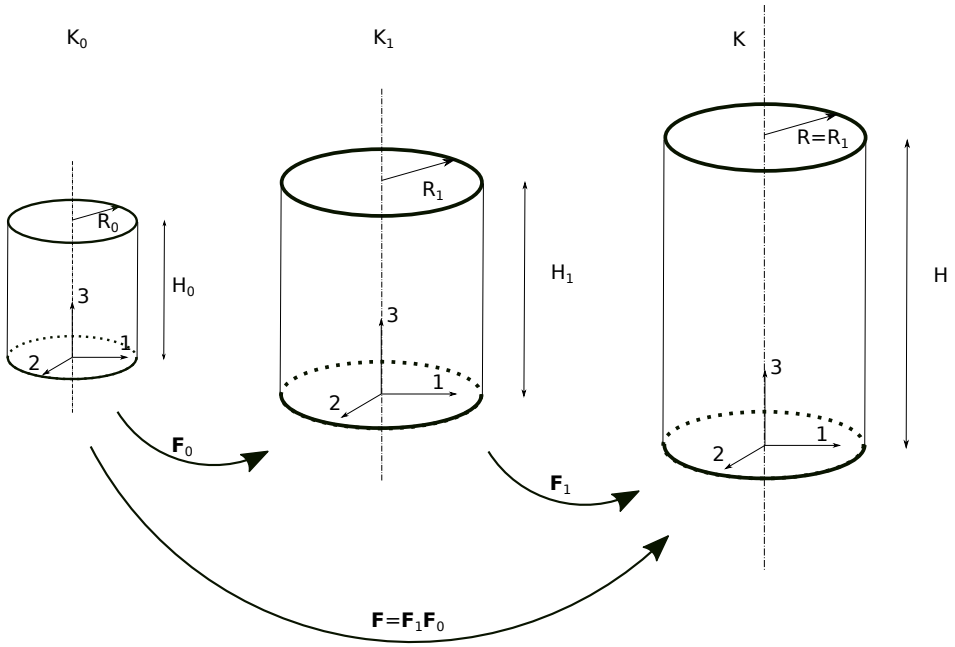

Figure 5: Illustration of uniaxial swelling of a circular cylindrical hydrogel. Configuration K_0 is the dry state. K_1 is the initial equilibrium configuration in which the hydrogel is in an isotropic state of strain. K is current configuration in which the gel undergoes uniaxial swelling.

This then leads to the following expression for the chemical potential:

$$\mu = k_B T \left(\ln \left(\frac{{\lambda_0}^3 \lambda - 1}{{\lambda_0}^3 \lambda} \right) + \frac{1}{{\lambda_0}^3 \lambda} + vN \left(\frac{\lambda}{\lambda_0} - \frac{1}{{\lambda_0}^3 \lambda} \right) + \frac{\chi}{{\lambda_0}^6 \lambda^2} \right). \tag{39}$$

In this example, we assume that the chemical potential remains constant at all times. However, at a given particle in the gel the stretch is a function of time and, the crosslink density N is also varying with time due to the opening of some crosslinks. Using eq.(39), this leads to the following evolution equation for λ:

$$\frac{\partial \lambda}{\partial t} = \frac{-v \frac{\partial N}{\partial t} (\frac{\lambda}{\lambda_0} - \frac{1}{\lambda_0^3 \lambda})}{\frac{1}{\lambda_0^3 \lambda^2 - \lambda} - \frac{1}{{\lambda_0}^3 \lambda^2} + vN \left(\frac{1}{\lambda_0} + \frac{1}{{\lambda_0}^3 \lambda^2} \right) - 2 \frac{\chi}{{\lambda_0}^6 \lambda^3}}. \tag{40}$$

In the coordinate system, described in Figure 5, the mobility tensor $\mathbf{M}$ in eq.(12) has the following matrix representation:

$$\mathrm{M} = D \begin{bmatrix} 1/\lambda_0^2 & 0 & 0 \\ 0 & 1/\lambda_0^2 & 0 \\ 0 & 0 & 1/(\lambda_0^2 \lambda^2) \end{bmatrix}. \tag{41}$$

In this example, the stretch λ and the different concentrations are functions of time and the longitudinal coordinate. In the dry configuration K_0, we define the normalized coordinate $\overline{X}_3 = X_3/H_0$ where X_3 is the Lagrangian longitudinal coordinate and H_0 the height of the gel. Note that $H_1 = \lambda_0 H_0$. The conservation equation for the target subject to reaction and diffusion within this cylindrical gel in K_0 is derived from eq.(7):

$$\frac{\partial C(\overline{X}_3, t)}{\partial t} = \frac{\partial}{\partial \overline{X}_3} \left(\frac{D}{H_1^2 \lambda^2} \frac{\partial C(\overline{X}_3, t)}{\partial \overline{X}_3} \right) + s(\overline{X}_3, t) J(\overline{X}_3, t), \quad 0 \leq \overline{X}_3 \leq 1 \tag{42}$$

Therefore, eqs.(42) and (18) and the following partial differential equations describe the coupled problem between swelling and diffusion-reaction in the cylinder along its longitudinal direction:

$$s = -k^+ \frac{C}{\lambda\lambda_0^3} m_t + k^+ \frac{C}{\lambda\lambda_0^3} m_c + k^+ \frac{C}{\lambda\lambda_0^3} m_0 + k^- m_c \tag{43}$$

$$\frac{\partial m_c}{\partial t} = k^+ \frac{C}{\lambda\lambda_0^3} m_t - k^+ \frac{C}{\lambda\lambda_0^3} m_c - k^+ \frac{C}{\lambda\lambda_0^3} m_0 - k^- m_c - k_b m_c \tag{44}$$

$$\frac{\partial m_0}{\partial t} = k_b m_c \tag{45}$$

$$\frac{\partial \lambda}{\partial t} = \frac{-v\frac{\partial N}{\partial t}\left(\frac{\lambda}{\lambda_0} - \frac{1}{\lambda_0^3\lambda}\right)}{\frac{1}{\lambda_0^3\lambda^2-\lambda} - \frac{1}{{\lambda_0}^3\lambda^2} + vN\left(\frac{1}{\lambda_0} + \frac{1}{{\lambda_0}^3\lambda^2}\right) - 2\frac{\chi}{{\lambda_0}^6\lambda^3}}. \tag{46}$$

Figure 6 shows $\frac{H}{H_1}$ against $\frac{tD}{H_1^2}$ computed with our FE implementation and with Matlab pdepe solver.

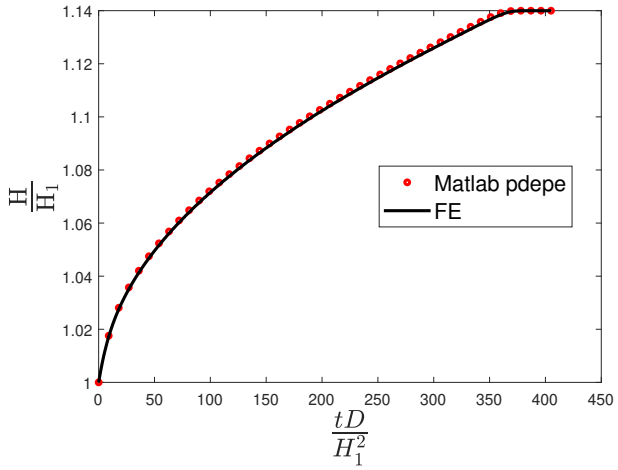

Figure 6: $\frac{H}{H_1}$ against dimensionless time $\frac{tD}{H_1^2}$ obtained using the pdepe Matlab (circles) function and the FE element solver `ABAQUS` (solid lines) against time.

As can be seen, the two analyses are in good agreement. At $\frac{tD}{H_1^2} = 365$ the concentration of the open complex m_0 is homogeneous and thus the cylinder has reached a new equilibrium with a homogeneous state of strain characterized in this example by $\lambda = 1.14$ at any particle in the gel. The two analyses are in excellent agreement with respect to this value.

3.3 Influence of swelling on the reaction-diffusion process

The reaction-diffusion process of target T into the hydrogel described by eqs.(5) and (6) is dependent on the current configurations K, i.e. the deformations of the gel. In order to investigate the influence of the deformations due to swelling and mechanical constrained that can be imposed to some part of the gel, we run three FE simulations of a hemi-spherical hydrogel. To this end, we used an axisymmetric FE model shown in Figure 7. The vertical edge of the gel is the axis of symmetry. Initially, the gel is at equilibrium in configuration K_1 and submerged in an external solution with a concentration of free targets $c = 0$. Only the outer edge marked with the purple dashed line (see Figure 7a) is in contact with the external solution. The horizontal edge marked with the white dotted line is in contact with a rigid

optical fiber. Hence, the nodes along the white dotted horizontal line are constrained in the 2-direction. Therefore, in K_1 the height of the gel is L_1 and its radius is R_1. At time $t = 0$, the concentration of the free target at the outer surface is increased to $c = c_{out}$ and the reaction diffusion process takes place and the gel starts to swell with a current height l.
In the first analysis, deformations are not considered and consequently the gel does not change in dimensions. In the second analysis, the crosslink term N is dependent on the open crosslink concentration as described in eqs.(16) and (17). Therefore, in the analysis the gel is swelling maintaining its hemispherical shape with a current height $l = l_f(t)$ (see Figure 7c). We call this case "Swelling without constraint". In the third analysis, the crosslink term N is still defined by eqs.(16) and (17) and in addition, the nodes in contact with the optical fiber (horizontal white dotted line in Figure 7a) are also constrained in the 1-direction. We call this case "Swelling with constraints". Thus, the length of this edge remains constant during the analysis and the current height of the gel is defined as $l_c(t)$, Figure 7d.
The color plots in Figures 7b-d depict the concentration m_0 of open crosslinks inside the gel at time $t =$ 5400 s.
We define the material coordinate X_2 in the initial configuration K_1. For Points O and A defined in Figure 7a, $X_2 = 0$ and $X_2 = L_1$, respectively. We also defined the normalized material coordinate $\bar{X}_2 = \frac{X_2}{L_1}$. Additionally, we define the current coordinate x_2 in the current configuration K such as $x_2 = 0$ and $x_2 = l(t)$ at Points O and A, respectively. We also defined the normalized current coordinate $\bar{x}_2 = \frac{x_2}{l(t)}$. Except for Points O and A, $\bar{X}_2 \neq \bar{x}_2$ because swelling develops locally. Note that in our experimental setup, the acquisition of the spatial distribution of the target is achieved with respect to the current coordinate x_2 as it is not possible to track particles. However, with the FE method used herein, it is more natural to use X_2.
In Figures 8a-b, the total concentration $(c + m_c + m_0)$ against time is presented at different locations along the vertical edge of the gel defined in terms of the normalized spatial coordinate $\bar{x}_2$ and the normalized material coordinate $\bar{X}_2$, respectively. These results illustrate the influence of swelling on the response of the reaction-diffusion model. The reaction-diffusion process is faster in the case when swelling is ignored and slowest when swelling is accounted for but without constraint. The difference between the three cases is increasing as the output locations get closer to the optical fiber. The spatiotemporal distribution of the concentration is very similar when using the normalized coordinates $\bar{X}_2$ or $\bar{x}_2$.
In Figure 9, the volume fraction of the polymer inside the hydrogel φ is plotted against time at different locations along the vertical edge of the finite element model for the cases "swelling without constraint" and "swelling with constraints". As can be seen, the volume fraction of the polymer φ is constant after $t \approx 9000$ s in both cases. φ reaches an homogeneous value for the case "swelling without constraint" of 0.031. However, in the case "swelling with constraint", the final φ field is inhomogeneous: the minimum value of φ is 0.030 at Point A and increases towards Point O to 0.037.
In addition, Figure 9 shows that swelling induces an inhomogeneous response with respect to the volume fraction of the polymer φ. Besides, mechanical constraints due to the optical fiber lead to a final inhomogeneous distribution of φ. These inhomogeneities are due to local swelling. As the diffusion coefficient D of the target T in the gel may be dependent on the polymer volume fraction (see Section 2.2.4), it emphasizes the importance of accounting for both swelling and mechanical constraints in the reaction-diffusion model. To this end, the FE method is well suited.

3.4 Influence of initial geometry

In the Section 3.3, the influence of swelling and mechanical constraints is illustrated on an initially hemispherical geometry, i.e $L_1 = R_1$ (see Figure 7). We now investigate the influence of the initial ratio

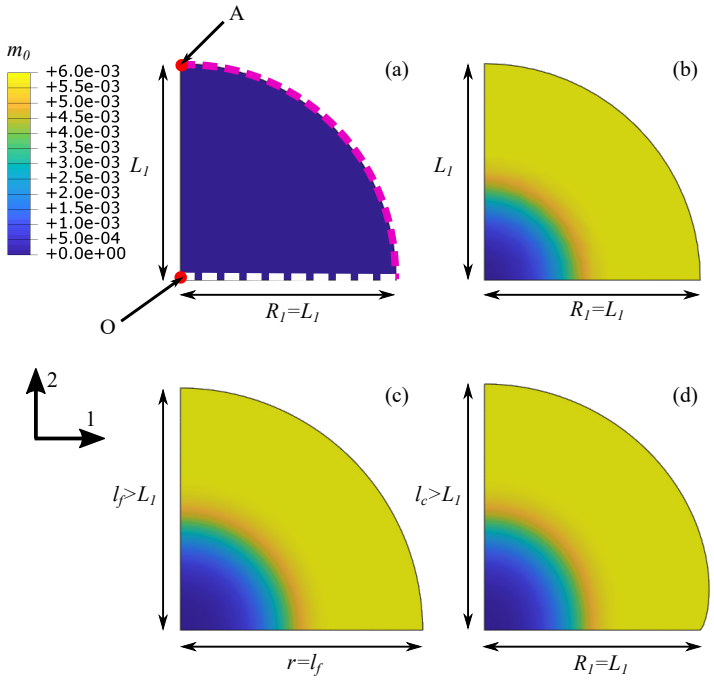

Figure 7: concentration m_0 (M) of open crosslinks inside an hemi-spherical gel (a) at time $t = 0$ s, (b) at time $t = 5400$ s without deformation, (c) at time $t = 5400$ s the case "Swelling without constraint", (d) at time $t = 5400$ s the case "Swelling with constraints".

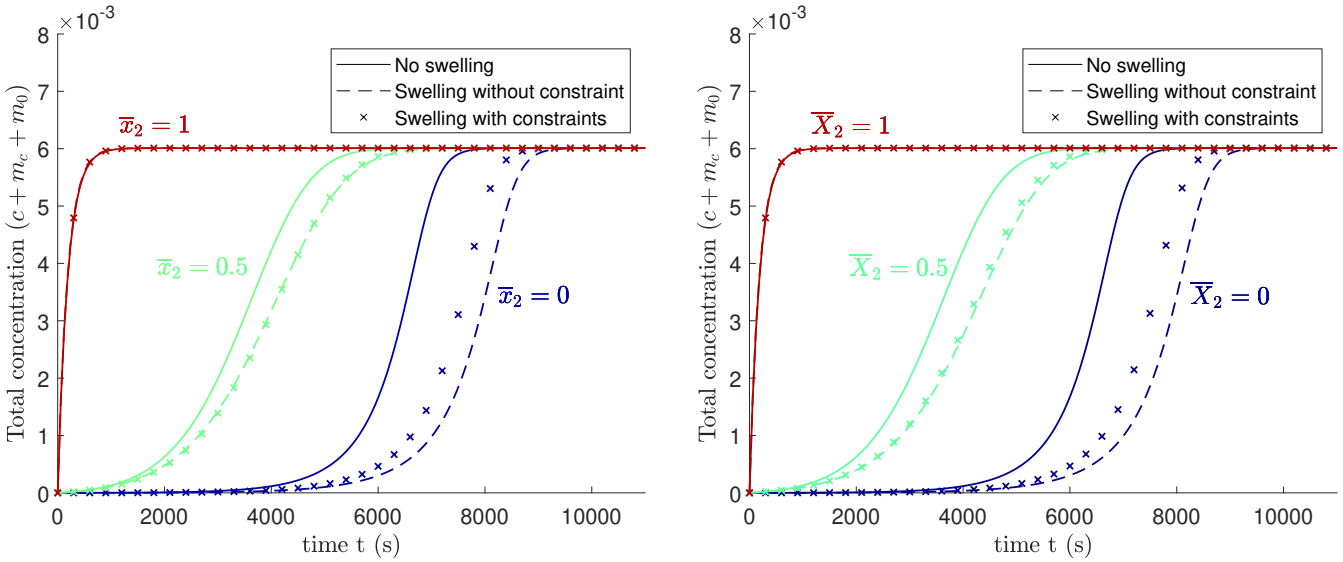

Figure 8: Total concentration (c+m_c+m_0) in M against time at three different locations: (a)$\bar{x}_2 = 1$, $\bar{x}_2 = 0.5$, $\bar{x}_2 = 0$, (b) $\bar{X}_2 = 1$, $\bar{X}_2 = 0.5$, $\bar{X}_2 = 0$.

$a = \frac{L_1}{R_1}$. Three analyses are run with the following ratios a 0.75, 1 and 1.25. Thus, the initial geometries are hemi-spheroidal for $a \neq 1$. The material properties, boundary and initial conditions are the same as

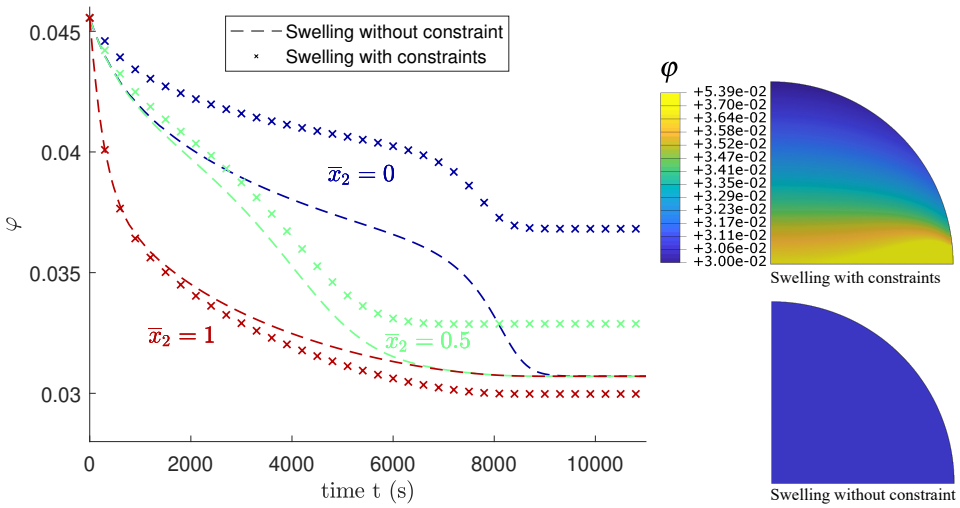

Figure 9: Volume fraction of the polymer inside the hydrogel φ at three different locations ($\bar{x}_2 = 1$, $\bar{x}_2 = 0.5$, $\bar{x}_2 = 0$) along the vertical edge against time t for the cases "swelling without constraint" (dashed lines) and "swelling with constraints" (crosses). Two snapshots of the FE analyses of the corresponding cases are included on the right at t=11000s.

for the case "swelling with constraints" from Section 3.3. Therefore, the radius of the gel R_1 is constant during the analyses while its height is varying and denoted l_c in the current configuration K. The total

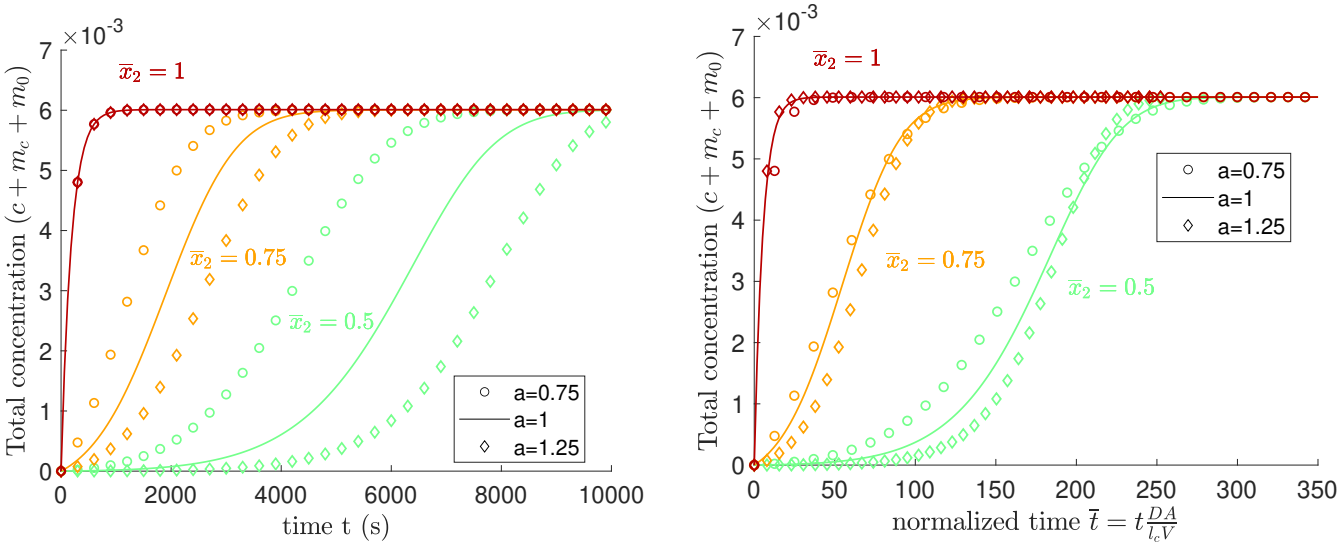

(a) (b)

Figure 10: Total concentration $(c + m_c + m_0)$ in M at three different locations ($\bar{x}_2 = 1$, $\bar{x}_2 = 0.75$, $\bar{x}_2 = 0.5$) for three different ratio $a = \frac{L_1}{R_1}$ (see Figure 7) , (a) against time, (b) against normalized time.

concentration $(c + m_0 + m_c)$ is plotted in Figures 10a and b against time t and against normalized time $\bar{t}$, respectively, for the three cases at different location along the vertical edge of the gel. The normalized time $\bar{t}$ is calculated as: $\bar{t} = t\frac{DA}{l_c V}$, where A is the initial outer area of the gel in contact with the external solution and V its initial volume. Figure 10a shows that oblate and prolate spheroidal geometries lead

to different concentration responses along their axis of revolution. These differences can be somewhat attenuated by using a normalized time scale (see Figure 10b). Experimentally, idealized shapes may be difficult to fabricate. Therefore, the FE method can be a valuable tool as it can account for various types of geometries.

4 Modeling reaction-diffusion in DNA and Morpholino hydrogels

Our reaction-diffusion model is fitted to four kinds of hydrogels, SB gels, CoumSB, SBF and Morpholino hydrogels (see Section 2.3) by means of an inverse FE technique. The FE model used in the fitting procedure is similar to the model "Swelling with constraints" described in Section 3.3. R_1 is assumed equal to the radius of the optical fiber on which the hydrogels are bounded, 62.5 μm. However, the initial height of the gels L_1 are obtained from experimental measurements and thus $L_1 \neq R_1$.
In all cases, the initial polymer fraction φ is taken equal to 0.06 as estimated during experiments. Therefore, all FE simulations starts in K_1 (see Figure 2) with a deformation gradient $\mathbf{F} = \mathbf{F_0} = \lambda_0 \mathbf{1}$ with $\lambda_0 = 2.554$.
For each case, the dimensionless number Nv (see eq.(4)) is adjusted so that the final heights of the gel l_c in the simulations correspond to the ones measured during experiments. We assumed that the crosslink term, N, consists of two contributions (see eq.(16)). N_{bis} is assumed to be constant and in Configuration K_1, $N_{dsDNA} = \frac{2}{3} N_{bis}$.
The value of $\frac{\mu}{k_B T}$ (see eq.(4)) is computed such as $\boldsymbol{\sigma} = \mathbf{0}$ in K_1. The parameters m_t, k^+, k^-, k_b and D (see Section 2.2.2) are estimated by minimizing the difference between the experimental and numerical total concentration $(c + m_c + m_0)$ profiles along the vertical edge of the gel, i.e., from $x_2 = 0$ to $x_2 = l_c(t)$ at different instant of time. The minimization is performed with a nonlinear least square technique using the *lsqnonlin* MATLAB function. Note that in this section, the diffusion parameter D is a function of the polymer volume fraction φ given by eq.(19).
In all simulations, at time $t = 0$ s, the target concentration c_{sol} in the external solution is assumed equal to 20 μM as described in the methods. Therefore, the concentration c_{out} at the boundary of the gel in contact with the external solution (purple dashed line in Figure 7a) is given by the relation $c_{out} = K_{\mathrm{TX}} c_{sol}$ where K_{TX} is the partition coefficient of the Target TX.
The comparison between the experimental and obtained FE total concentration $(c + m_c + m_0)$ profiles along the vertical edge of the gel is shown in Figures 11 and 12 for CoumSF and morpholino gels. Additional comparisons are provided in Figure S1 in Supplementary for SB and SBF gels. The corresponding fitted parameters are reported in Table 2. As can be seen, the FE simulations are in somewhat good agreement with the experimental data. For the morpholino gel with Target T10 (Figure 12b), the reaction-diffusion process happens too quickly in the simulation compared to the experimental results after 600 s. For the gel CoumSB T3 (Figure 11a), the slope of the concentration profile is overestimated by the simulations until 1000 s. The FE simulations are in best agreement with the experimental data in the central regions of the concentration slopes. The peak observed in the experimental data at low values of x_2, i.e. near the fiber end face, such as in Figure 11a is caused by the procedure used to correct for the loss of fluorescence due to the presence of the fibre, as discussed in section 2.3. Furthermore, the maximum concentration reached within the hydrogel, as observed from the experimental data, is not constant throughout the hydrogel, as would be expected at equilibrium based on the design of the system, but is often observed to decline at the outer edge of the hydrogel. While a nearly step-change in the total concentration $(c + m_c + m_0)$ of target DNA could be expected when extending from a homogeneous gel to the immersing solution, there is some smoother transition as imaged via CLSM with a nonzero confocal volume. Nevertheless, the less pronounced decline at the hydrogel - immersing solu-

Table 2: Estimated parameters used in the simulations presented in Section 4. The parameters in shaded grey are those determined from the inverse FE procedure. Note that the diffusion parameter D is provided for the initial polymer volume fraction $\varphi = 0.06$.

Gel type		reaction-diffusion parameters						crosslink term		gel height (μm)	
		$D_{\lvert\varphi=0.06}$ (μm^{2}s^{-1})	k^+ (M^{-1}s^{-1})	k^- (s^{-1})	k_b (s^{-1})	$m_t(M)$	K_{TX}	$N_{bis}v$	γ	initial (L_1)	final (l_c)
SB	T7	43	5.9e+4	8.8e−3	0.01	1.3e−4	0.20	0.0011	0.55	55.5	67.6
CoumSB	T3	30	1.4e+3	1.3e−5	6.9e+3	2.6e−4	0.14	0.000946	0.7	48.7	61.2
CoumSB	T7	26	2.0e+4	8.3e−6	1.4e+4	3.3e−4	0.14	0.00093	0.7	54.8	67.6
SBF	T7	40	3.2e+4	4.2e−8	1.e+5	3.3e−4	0.079	0.00094	0.7	53.2	65.8
SBF	T3	22	2.1e+3	3.3e−7	334	2.0e−4	0.079	0.00106	0.55	57.9	68.8
Morpholino	T2	5.0	317	1.0e−2	0.01	5.3e−5	0.78	0.0018	0.05	77.8	79.5
Morpholino	T10	9.9	1.5e+3	7.9e−4	3.1	1.6e−4	0.78	0.0022	0.05	80.0	82.0

tion boundary is not straightforward to explain. Possible factors contributing to this include e.g. non-constant concentration of the target in the hydrogel due to a non-constant concentration of the binding sites, as caused by inhomogeneities in concentration during preparation (such as of the oligonucleotides or the photoinitiator, the latter possible arising from the use of photoinitiator in the immersing oil in the preparation step), or changes to the concentration of the binding sites as a result of the local swelling. In Table 3, the parameters estimated from our previous studies[47,48] are reported. These parameters were estimated by approximating the gel geometries as hemi-spherical and ignoring fiber constraints and swelling. Ignoring these effects lead to lower values for the diffusion parameter except for the morpholino gels. For the morpholino gels, swelling was quite limited as can be seen from the gel heights reported in Table 2. And thus, the mechanical constraints due the fiber are also reduced. In this case, a simpler approach as the one described in Section 3.1 may be satisfactory. However, such an approach does not take into account the geometrical effects described in Section 3.4.

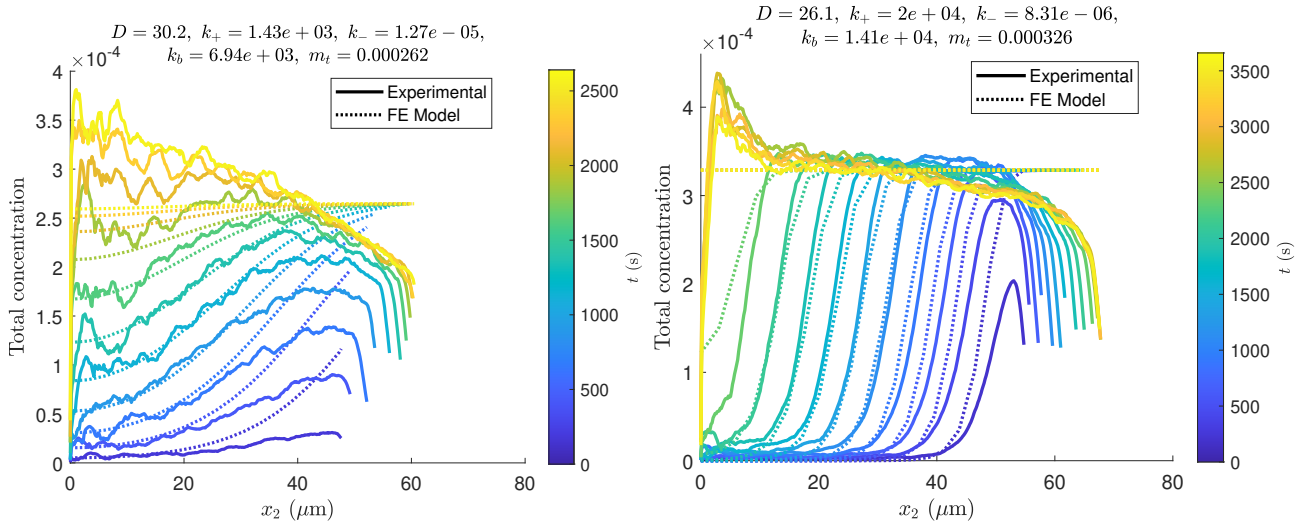

(a) CoumSB T3 (b) CoumSB T7

Figure 11: Comparison between the experimental and obtained FE total concentration ($c + m_c + m_0$) (M) profiles along the vertical edge of the gel for the CoumSB gels a) CoumSB T3, b) CoumSB T7. The edge of the fibre is positioned at $x_2 = 0$ and the outer edge of the swelling gel is seen at the right.

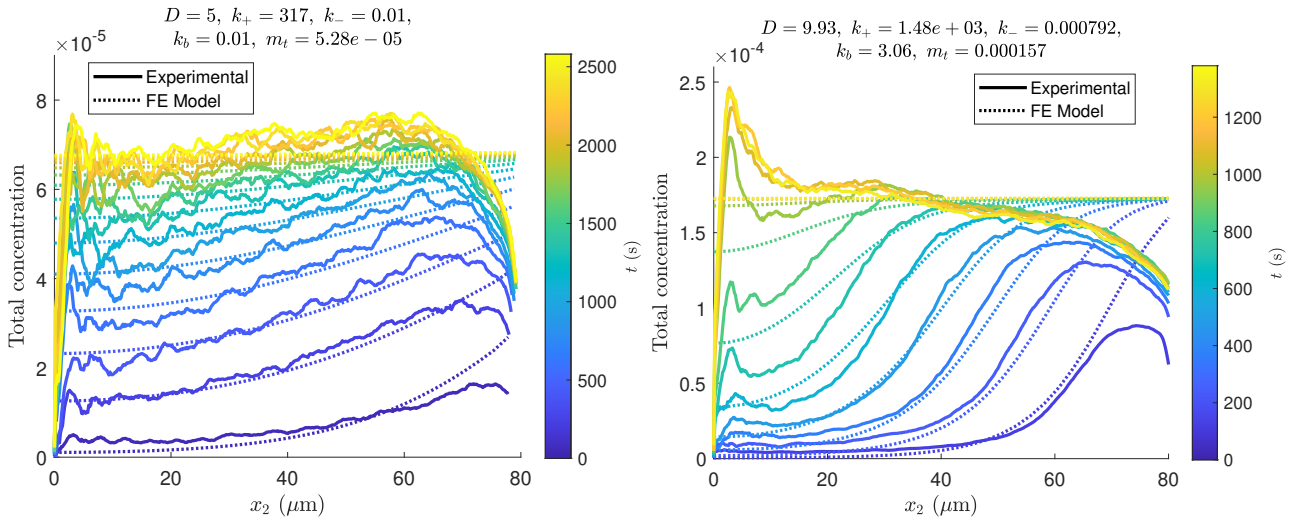

(a) Morpholino T2

(b) Morpholino T10

Figure 12: Comparison between the experimental and obtained FE total concentration $(c+m_c+m_0)$ (M) profiles along the vertical edge of the gel for the Morpholino gels a) Morpholino T2, b) Morpholino T10. The edge of the fibre is positioned at $x_2 = 0$ and the outer edge of the swelling gel is seen at the right.

Table 3: Estimated parameters from previous studies[47,48]

Gel type		reaction-diffusion parameters				
		D (μm^{2}s^{-1})	k^+ (M^{-1}s^{-1})	k^- (s^{-1})	k_b (s^{-1})	$m_t(M)$
SB	T7	21.9	3.96e+4	7.93e−5	1.99	1.18e−4
CoumSB	T3	24.2	1.09e−3	6.03e−3	3.71	2.25e−4
CoumSB	T7	26.6	1.89e−4	2.78e−7	0.56	3.19e−4
SBF	T7	35.5	4.84e+4	1.94e−3	2.21	3.31e−4
SBF	T3	17.8	1.68e+3	8.75e−2	2.39	1.72e−4
Morpholino	T2	-	-	-	-	-
Morpholino	T10	11.8	2.5e+3	0.95	2.8	1.4e−4

5 Conclusion

In this work, we propose a finite element approach to model reaction-diffusion processes in DNA-reactive hydrogels. Our modeling approach is capable to account for various geometries, constraints and swelling of the gels. The numerical examples presented in this study show that these aspects need to be accounted for in order to better evaluate the parameters of the reaction model. Finally, the numerical method is applied to DNA and Morpholino hydrogels. The numerical results show a satisfying agreement with the experimental data and that this modeling approach is able to capture the effect induced by the use of different toehold of the target DNA.

The present work, where mechanistic details in a particular reaction-diffusion processes in molecular responsive hydrogels are included in the finite element framework, could also serve to inspire similar approaches for other mechanisms. Examples of this include cas12 digestion of DNA strands in hydrogels[12] thus inducing decreased crosslink density, or enzyme catalyzed increased crosslinking[50]. It should also be noted that similar strategies can be applied also for the coupled phenomena when enzyme induced

degradation of the extracellular matrix by cell secreted enzymes are integrated in a model[51,52]. In these examples, the representation of the molecular mechanism of the molecular specie triggering the network structural changes can be different from the present work, and need to be changed accordingly in their modeling representation.

Author contributions

Conceptualization, E.P.J., B.T.S., V.P.; Methodology, V.P.; Investigation, E.P.J., V.P..; Software V.P.; Visualization E.P.J, V.P.; Supervision, B.T.S., V.P.; writing, original draft preparation, E.P.J., B.T.S., V.P.; writing – review and editing, E.P.J., B.T.S., V.P. All authors have read and approved the final version of the manuscript.

Conflicts of interest

There are no conflicts of interest to declare.

References

1 R. Barbucci, *Hydrogels: Biological properties and applications*, Springer Science & Business Media, 2010.

2 M. A. C. Stuart, W. T. S. Huck, J. Genzer, M. Muller, C. Ober, M. Stamm, G. B. Sukhorukov, I. Szleifer, V. V. Tsukruk, M. Urban, F. Winnik, S. Zauscher, I. Luzinov and S. Minko, *Nature Materials*, 2010, **9**, 101–113.

3 A. Doering, W. Birnbaum and D. Kuckling, *Chemical Society Reviews*, 2013, **42**, 7391–7420.

4 R. V. Ulijin, N. Bibi, V. Jayawarna, P. D. Thornton, S. J. Todd, R. J. Mart, A. M. Smith and J. E. Gough, *Materials Today*, 2007, **10**, 40–48.

5 M. Karbarz, M. Mackiewicz, K. Kaniewska, K. Marcisz and Z. Stojek, *Applied Materials Today*, 2017, **9**, 516–532.

6 P. Sikdar, M. M. Uddin, T. M. Dip, S. Islam, M. S. Hoque, A. K. Dhar and S. Y. Wu, *Materials Advances*, 2021, **2**, 4532–4573.

7 T. Miyata, N. Asami and T. Uragami, *Nature*, 1999, **399**, 766–769.

8 S. L. Lim, C. W. Ooi, W. S. Tan, E. S. Chan, K. L. Ho and B. T. Tey, *Sensors and Actuators B-Chemical*, 2017, **252**, 409–417.

9 J. J. Qin, X. Q. Li, L. X. Cao, S. B. Du, W. Wang and S. Q. Yao, *Journal of the American Chemical Society*, 2020, **142**, 417–423.

10 T. Miyata, M. Jige, T. Nakaminami and T. Uragami, *Proc. Natl. Acad. Sci. U. S. A.*, 2006, **103**, 1190–1193.

11 K. M. Schultz, K. A. Kyburz and K. S. Anseth, *Proceedings of the National Academy of Sciences of the United States of America*, 2015, **112**, E3757–E3764.

12 M. A. English, L. R. Soenksen, R. V. Gayet, H. de Puig, N. M. Angenent-Mari, A. S. Mao, P. Q. Nguyen and J. J. Collins, *Science*, 2019, **365**, 780–785.

13 J. H. Holtz, J. S. W. Holtz, C. H. Munro and S. A. Asher, *Analytical Chemistry*, 1998, **70**, 780–791.

14 S. Tierney, S. Volden and B. T. Stokke, *Biosensors and Bioelectronics*, 2009, **24**, 2034–2039.

15 C. J. Zhang, G. G. Cano and P. V. Braun, *Advanced Materials*, 2014, **26**, 5678–5683.

16 K. Barker, S. K. Rastogi, J. Dominguez, T. Cantu, W. Brittain, J. Irvin and T. Betancourt, *Journal of Biomaterials Science, Polymer Edition*, 2016, **27**, 22–39.

17 D. Wang, Y. Hu, P. Liu and D. Luo, *Accounts of Chemical Research*, 2017, **50**, 733–739.

18 V. Morya, S. Walia, B. B. Mandal, C. Ghoroi and D. Bhatia, *Acs Biomaterials Science & Engineering*, 2020, **6**, 6021–6035.

19 R. V. Gayet, H. de Puig, M. A. English, L. R. Soenksen, P. Q. Nguyen, A. S. Mao, N. M. Angenent-Mari and J. J. Collins, *Nature Protocols*, 2020, **15**, 3030–3063.

20 N. A. Peppas, J. Z. Hilt, A. Khademhosseini and R. Langer, *Advanced Materials*, 2006, **18**, 1345–1360.

21 I. Minrath, D. Arbeiter, K. P. Schmitz, K. Sternberg and S. Petersen, *Polymers for Advanced Technologies*, 2014, **25**, 1234–1241.

22 M. Shibayama and T. Tanaka, *Advances in Polymer Science*, 1993, **109**, 1–62.

23 S. Nagahara and T. Matsuda, *Polymer Gels and Networks*, 1996, **4**, 111–127.

24 E. J. Cheng, Y. Z. Xing, P. Chen, Y. Yang, Y. W. Sun, D. J. Zhou, L. J. Xu, Q. H. Fan and D. S. Liu, *Angewandte Chemie-International Edition*, 2009, **48**, 7660–7663.

25 C. H. Lu, W. W. Guo, Y. W. Hu, X. J. Qi and I. Willner, *Journal of the American Chemical Society*, 2015, **137**, 15723–15731.

26 F. Li, J. Tang, J. Geng, D. Luo and D. Yang, *Progress in Polymer Science*, 2019, **98**, 101163.

27 A. G. Thombre and K. J. Himmelstein, *AIChE Journal*, 1985, **31**, 759–766.

28 A. Joshi and K. J. Himmelstein, *Journal of Controlled Release*, 1991, **15**, 95–104.

29 J. Siepmann and A. Göpferich, *Advanced Drug Delivery Reviews*, 2001, **48**, 229–247.

30 S. Lyu, R. Sparer and D. Untereker, *Journal of Polymer Science Part B: Polymer Physics*, 2005, **43**, 383–397.

31 A. N. Versypt, P. D. Arendt, D. W. Pack and R. D. Braatz, *PLoS ONE*, 2015, **10**, e0135506.

32 M. Parlato and W. Murphy, *Hydrogels in Cell-Based Therapies*, The Royal Society of Chemistry, 2014, pp. 1–30.

33 W. Hong, X. Zhao, J. Zhou and Z. Suo, *Journal of the Mechanics and Physics of Solids*, 2008, **56**, 1779–1793.

34 W. Hong, Z. Liu and Z. Suo, *International Journal of Solids and Structures*, 2009, **46**, 3282–3289.

35 M. K. Kang and R. Huang, *Journal of Applied Mechanics*, 2010, **77**, 61004.

36 W. Toh, Z. Liu, T. Y. Ng and W. Hong, *International Journal of Applied Mechanics*, 2013, **05**, 1350001.

37 P. J. Flory, *Principles of polymer chemistry*, Cornell University Press, 1953.

38 M. L. Huggins, *The Journal of Chemical Physics*, 1941, **9**, 440–440.

39 P. J. Flory, *The Journal of Chemical Physics*, 1942, **10**, 51–61.

40 Abaqus, *6.14-4*, Dassault Systèmes, 2014.

41 N. R. Richbourg and N. A. Peppas, *Progress in Polymer Science*, 2020, **105**, 101243.

42 H. Yasuda, C. E. Lamaze and L. D. Ikenberry, *Die Makromolekulare Chemie*, 1968, **118**, 19–35.

43 L. Johansson, U. Skantze and J. E. Löfroth, *Macromolecules*, 1991, **24**, 6019–6023.

44 B. Amsden, *Macromolecules*, 1998, **31**, 8382–8395.

45 R. I. Cukier, *Macromolecules*, 1984, **17**, 252–255.

46 E. Stellwagen, Y. J. Lu and N. C. Stellwagen, *Biochemistry*, 2003, **42**, 11745–11750.

47 E. P. Jonášová, A. Bjørkøy and B. T. Stokke, *Biomacromolecules*, 2020, **21**, 1698–1699.

48 E. Parelius Jonášová and B. T. Stokke, *Polymers*, 2020, **12**, 268.

49 E. P. Jonášová, A. Bjørkøy and B. T. Stokke, *Journal of Biomedical Optics*, 2016, **21**, 126014.

50 W. Song, J. Ko, Y. H. Choi and N. S. Hwang, *APL Bioengineering*, 2021, **5**, 021502.

51 V. Dhote and F. J. Vernerey, *Biomechanics and Modeling in Mechanobiology*, 2014, **13**, 167–183.

52 M. C. Schneider, S. Lalitha Sridhar, F. J. Vernerey and S. J. Bryant, *Journal of Materials Chemistry B*, 2020, **8**, 2775–2791.